AIP | Review of Scientific Instruments

Attosecond beamline with actively stabilized and spatially separated beam paths

M. Huppert, I. Jordan, and H. J. Wörner

Citation: Review of Scientific Instruments **86**, 123106 (2015); doi: 10.1063/1.4937623
View online: http://dx.doi.org/10.1063/1.4937623
View Table of Contents: http://scitation.aip.org/content/aip/journal/rsi/86/12?ver=pdfcov
Published by the AIP Publishing

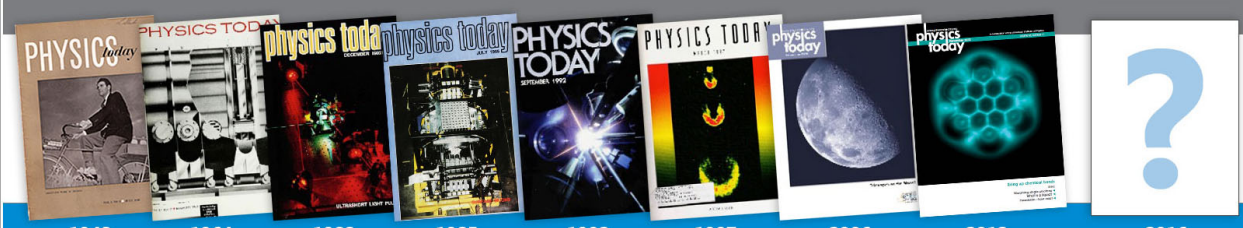

Attosecond beamline with actively stabilized and spatially separated beam paths

M. Huppert, I. Jordan, and H. J. Wörner[a)]
Laboratory of Physical Chemistry, ETH Zurich, Vladimir-Prelog-Weg 2, CH-8093 Zurich, Switzerland

(Received 16 September 2015; accepted 30 November 2015; published online 15 December 2015)

We describe a versatile and compact beamline for attosecond spectroscopy. The setup consists of a high-order harmonic source followed by a delay line that spatially separates and then recombines the extreme-ultraviolet (XUV) and residual infrared (IR) pulses. The beamline introduces a controlled and actively stabilized delay between the XUV and IR pulses on the attosecond time scale. A new active-stabilization scheme combining a helium-neon-laser and a white-light interferometer minimizes fluctuations and allows to control delays accurately (26 as rms during 1.5 h) over long time scales. The high-order-harmonic-generation region is imaged via optical systems, independently for XUV and IR, into an interaction volume to perform pump-probe experiments. As a consequence of the spatial separation, the pulses can be independently manipulated in intensity, polarization, and frequency content. The beamline can be combined with a variety of detectors for measuring attosecond dynamics in gases, liquids, and solids. © *2015 AIP Publishing LLC.* [http://dx.doi.org/10.1063/1.4937623]

I. INTRODUCTION

Over the past 15 years, attosecond science has evolved from studying the simplest atomic systems[1] to addressing relatively complex molecules[2] and solids.[3] This development has been supported by continuous improvements of the experimental methodologies, from laser development over pulse compression techniques to the design of sophisticated beamlines for pump-probe measurements. The key challenge in realizing attosecond measurements on complex systems is the simultaneous requirements on delay stability, selectivity, and tunability of the pump and probe processes. Tailoring the pump and probe pulses to the specific system under study requires the use of band-pass filters, attenuators, or wave plates. Improvements in signal-to-noise ratio are best achieved through single-shot acquisition techniques using choppers. Most of these requirements are best fulfilled by a spatial separation of the pump and probe beams which, however, makes the delay stability challenging.

The first described scheme, which is still widely used today, consists of a dual spherical mirror assembly.[4–6] The inner part, equipped with a multilayer coating, is used for spectral selection and reflection of the desired part of the extreme-ultraviolet (XUV) spectrum. The outer part serves to reflect the residual infrared (IR) pulse after high-harmonic generation (HHG). This scheme benefits from a high mechanical stability, but is limited in terms of selectivity and tunability, especially with respect to the IR pulse. The same limitation applies to approaches, which introduce the delay collinearly before the HHG process.[7–10] Another successful approach consists in splitting the IR pulse before HHG and recombining XUV and IR pulses after the generation.[2,11–16] This configuration offers a high flexibility but the long optical path lengths make the delay control challenging, since each optical element introduces additional vibrations and thermally induced drifts scale with the optical path length. Furthermore, a different scheme has been described that combines the advantages of the spatially separated XUV and IR paths with the stability of a compact setup.[17] It relies on separating the XUV and IR beams after HHG, reflecting the XUV off a multilayer mirror under 45° incidence and introducing the delay in the IR beam path.

In this article, we describe a new design of an attosecond beamline, which was guided by the following considerations. Control over the XUV spectrum and spectral phase with metal filters and variation of its intensity with an iris are desirable. Similarly, control over the IR polarization with wave plates, variation of the IR intensity with an iris, and the possibility to generate low-order harmonics in a second non-linear medium are of great use. This wishlist is best fulfilled by spatially separated beam paths. We realized the required deflection of the XUV beam using a sequence of four grazing-incidence reflections. Choosing diamond-like carbon as the mirror coating, we achieve a good, nearly flat reflectivity over a bandwidth greater than 100 eV. Separating the XUV and IR pulses after HHG, in high vacuum, provides a good passive stability, but a residual long-term drift of several hundred attoseconds remains. This limitation is removed by an active stabilization relying on an innovative combination of helium-neon and white-light interferometers to achieve an excellent delay stability.

This article is structured as follows: Section II describes the mechanical and optical setup of the attosecond beamline. Section III describes the active stabilization scheme. Section IV demonstrates the application of the beamline to the reconstruction of attosecond pulse trains. Section V summarizes this article and provides an outlook on future applications.

[a)]Electronic mail: hwoerner@ethz.ch.

II. EXPERIMENTAL SETUP

The presented apparatus generates attosecond pulses from a femtosecond infrared laser source, spatially separates the fundamental beam from the high-order harmonics, and recombines them with a well defined time delay. The whole setup is operated under high vacuum conditions (low 10^{-6} mbar), maintained by turbomolecular pumps. All pumps are vibrationally decoupled from the optical table and the vacuum chambers, using flexible bellows and rubber bushes. All optical elements inside the chambers are mounted on thick (25 mm–50 mm) aluminum breadboards, which at the same time serve as bottom flanges for the vacuum system. Those breadboards are directly clamped to the optical table (450 mm thickness). The setup is schematically shown in Figure 1 and described in detail in Secs. II A–II D.

A. Generation of XUV radiation

The generation of coherent extreme ultraviolet radiation in the range of 10 eV to 150 eV is achieved by high-order harmonic generation from intense, ultrashort laser sources.[18,19] The intense infrared laser pulse is focused into a noble-gas filled region which acts as nonlinear generation medium. Different geometries like semi-infinite[20] or finite gas cells and pulsed or continuous gas jets can be used to efficiently generate different harmonic orders. Semi-infinite gas cells are known to deliver a relatively high photon flux.[21] Therefore, a semi-infinite gas cell was designed, which is characterized and described in more detail in a different publication.[22] The fundamental laser beam is focused by an off-axis parabolic mirror (LT Ultra, $f = 250$ mm or $f = 470$ mm, 30°, protected Ag-coating) into the gas cell. A pinhole (0.5 mm diameter) around the focal point separates the generating gas from the following two differential pumping stages. The high-order harmonics are generated in the pressure gradient around the focus. To optimize the generation efficiency, the pinhole and therefore the pressure gradient can be translated along the beam propagation axis. The focus position stays fixed to preserve the imaging properties of the optical system, imaging the generation into the detection region.

Two differential pumping stages allow for a generation gas pressure of up to 100 mbar (typically 10 mbar) without affecting the pressure in the following vacuum system. The first differential pumping stage is pumped by a high-vacuum

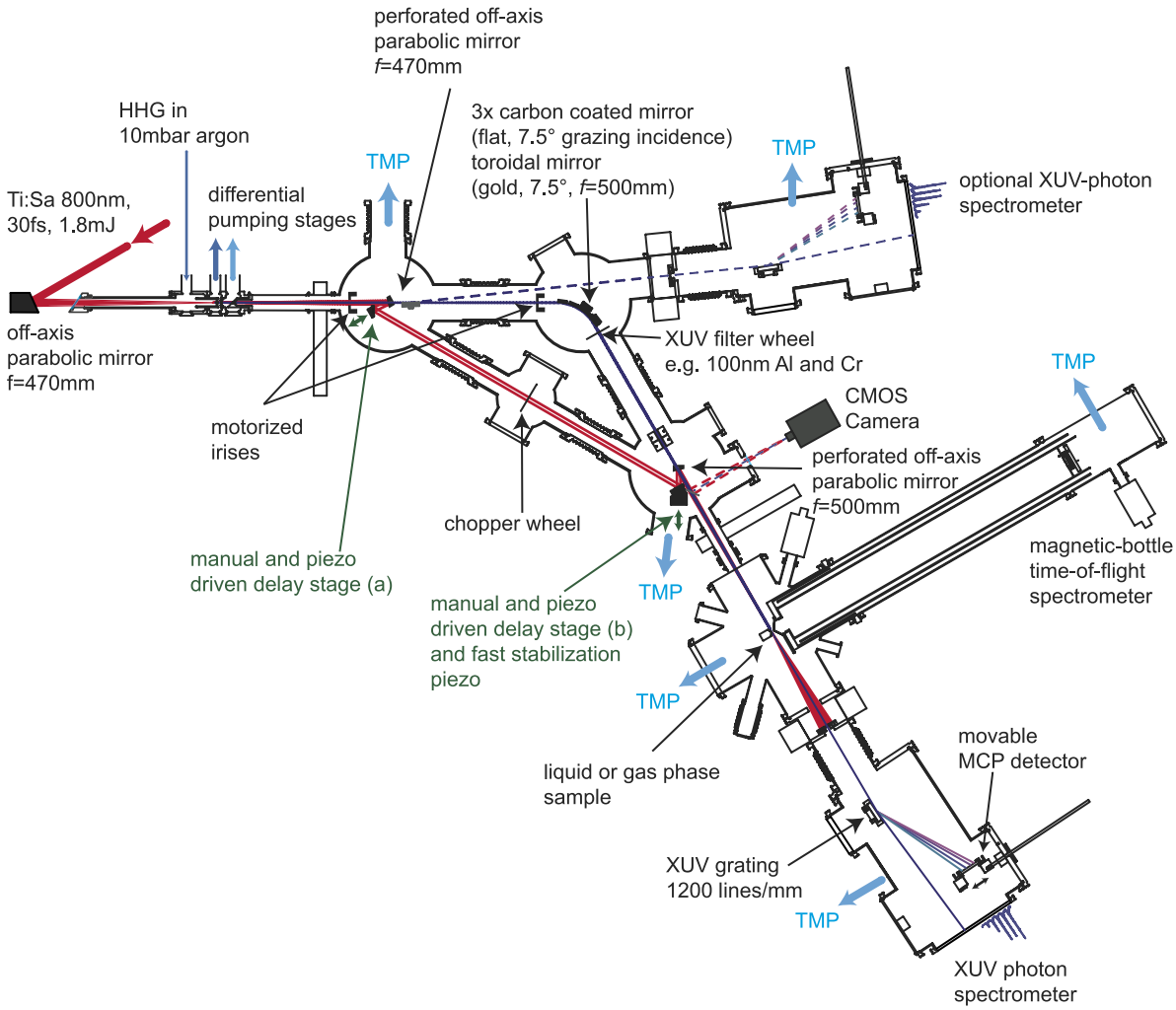

FIG. 1. Experimental setup: semi-infinite gas cell (HHG) (top left), delay generation (middle), magnetic-bottle time-of-flight spectrometer (bottom right) for pump-probe experiments, and an XUV photon spectrometer with two optional locations for diagnostics. Turbomolecular pumps are marked with TMP.

pump against atmosphere (Pfeiffer OnTool Booster 150, pumping speed: 130 m^3/h, ultimate pressure 10^{-5} mbar) which typically reaches $2 \cdot 10^{-2}$ mbar under gas load. In the second stage, a pressure of $3 \cdot 10^{-5}$ mbar is achieved using a turbomolecular pump. The gas cell, including the differential pumping stages, can be separated from the vacuum chambers hosting the delay generating elements using a gate valve. The whole gas cell assembly can be replaced by a different target, such as a finite gas cell or a pulsed valve, without changing subsequent optical elements, as long as the position of generation remains unchanged. The focal length is only restricted by the amount of power which is needed for the dressing beam, since it is recollimated by a 1 in. mirror standing 470 mm behind the point of generation.

B. Separation and delay generation

The delay line setup consists of four vacuum chambers which are connected by bellows. The fundamental and the XUV beams enter the first chamber co-linearly. As a consequence of the generation process, the XUV beam has a much lower divergence than the fundamental beam. A motorized iris can be used to attenuate the fundamental beam before it reaches the optics involved in the delay generation, which minimizes the thermal load on the mirrors and helps preventing drifts of the beam path length. The different divergence furthermore allows for the separation of the two beams with a perforated off-axis parabolic mirror (LT Ultra, $f = 470$ mm, 30°, protected Ag-coating). The XUV radiation is transmitted through a 2 mm hole, whereas the fundamental beam is reflected and at the same time recollimated. The recollimated beam is guided via two flat mirrors, which are mounted on two separate translation stages, onto the recombination mirror in the last vacuum chamber. Both stages (MRL80.25/FPSt150-5-140 Piezomechanik GmbH) can be translated by a micrometer screw (coarse) and by a piezoelectric actuator (fine) and are always moved synchronously to compensate changes to the beam pointing. The mirrors on the second stage are additionally mounted on a shorter range piezo (STr35/150/6 Piezomechanik GmbH), which allows fast movement for the active feedback loop. The recombination mirror is again a perforated (2 mm hole) off-axis parabolic mirror (LT Ultra, $f = 500$ mm, 30°, protected Ag-coating). The collimated beam between the two perforated mirrors can be modified in its properties (intensity, polarization state, frequency) without affecting the XUV beam. An optical chopper (Thorlabs MC2000) is used to block every second pulse of the fundamental laser beam, which allows for a shot-to-shot referencing of pump-probe experiments.

C. XUV beam path and diagnostics

The XUV beam passing through the first perforated mirror is propagating through a motorized iris onto a four-mirror assembly in the intermediate vacuum chamber. An overall deflection angle of 60° has been chosen to keep the whole setup compact. The spatially separated beam path has a length of about 1 m. For a reflection in the desired energy region between 10 eV and 150 eV, a trade-off between deflection angle, and therefore size of the setup, and overall reflectivity had to be found. We use four mirrors under 7.5° grazing incidence. Three of them are flat silicon substrates, coated with a thin layer of diamond-like carbon (50 nm to 100 nm, Ulrich Müller, EMPA). The carbon coating was chosen because it shows a high and almost flat reflectivity over the desired energy range. The fourth mirror is a gold-coated toroidal mirror (Optical Surfaces Ltd.), designed for 7.5° incidence angle and an effective focal length of $f = 500$ mm. The overall reflectivity shown in Fig. 2 is estimated from literature to lie between 25%[23] and 40%.[24] The reflectivity given by Henke is in good agreement with measurements performed in our laboratory on a different beamline[22] but does not cover energies below 30 eV. The values given by Hagemann extend to lower photon energies but are systematically lower than Henke's.

The spectrally averaged reflectivity for typical experimental conditions between 15 eV and 40 eV (11th to 27th harmonic of 800 nm generated in argon, see Fig. 2 green photoelectron (PE) spectrum) was measured with an aluminum-coated XUV-photodiode (Opto Diode Corp. AXUV100Al) for s- and p-polarization. The measured values are 29% for p-polarization and 55% for s-polarization (shown as red lines in Fig. 2), which is in good agreement with the literature, if the data by Henke are extrapolated below 30 eV using the qualitative behavior of Hagemann in this energy range. The measurement justifies the assumption that the reflectivity of the complete four-mirror assembly is around 40% for s-polarized radiation up to 120 eV.

Just as the fundamental beam, the XUV radiation can also be modified independently. An iris can be used to attenuate the XUV radiation and to suppress the long-trajectory contributions to the harmonics due to their larger divergence. A motorized filter wheel, hosting several few-hundred-nanometer thin metallic filters (Lebow Company), is used to suppress the residual fundamental light coming from the generation process through the perforated mirror. Furthermore, metals like tin, titanium, chromium, or indium[25] act as spectral bandpass filters[24,26,27] to select only a few

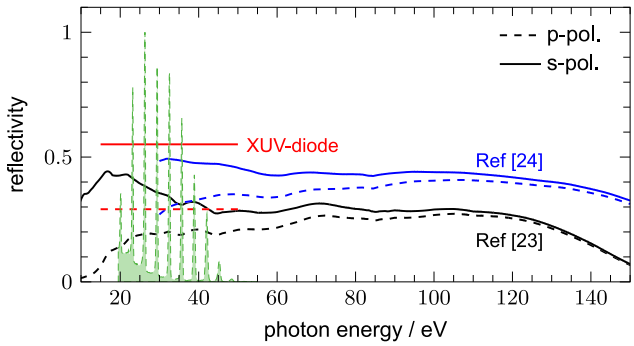

FIG. 2. Reflectivity of the XUV-mirror-assembly consisting of three carbon-coated and one gold-coated mirror under 7.5° grazing incidence. The reflectivity for s- and p-polarization (red and dashed red) is measured with our XUV-photodiode and compared to Henke[24] (blue) and Hagemann[23] (black). The experimental reflectivities are an average over the high harmonic spectrum which was generated from 800 nm in argon (experimental photoelectron spectrum shown in green).

high-order harmonics and influence the temporal profile of the attosecond pulses.[28]

The generated XUV radiation can be characterized using two ports to attach a home-built XUV-photon spectrometer based on a laminar type flat-field grating (Shimadzu, 30-002, 1200 grooves/mm). In the first vacuum chamber, directly behind the first perforated mirror, the beam can be directed under grazing incidence to the first diagnostics port. The other option is to connect the XUV-photon spectrometer behind the main interaction chamber, which allows synchronous detection of the on-target XUV spectrum and the generated photoelectrons.

The recombined beam can be picked off before entering the interaction chamber for alignment and diagnostic purposes. A camera is used for daily alignment of temporal and spatial overlap of the two beams, propagating the fundamental beam in both arms of the interferometer. The stability measurements presented in Sec. III C were recorded using a photodiode at this diagnostics port.

D. Interaction region

The XUV-generation region is imaged 1:1 into the interaction region. After the second perforated mirror XUV and fundamental radiation propagate collinearly, the foci are overlapping in all three spatial dimensions and the temporal delay between them can be adjusted. The interaction region can be separated from the rest of the beamline using a gate valve with an integrated window which allows for alignment of the detector under ambient-pressure conditions. A flexible bellow ensures that vibrations from the detector, which is mounted on a separate frame next to the optical table, are not coupled into the interferometric setup and onto the optical table. The frame of the detector can be moved in all three dimensions to align it with respect to the laser focus.

A wide variety of detectors (e.g. magnetic-bottle-time-of-flight spectrometer, velocity-map-imaging spectrometer, high-resolution-XUV spectrometer) is compatible with our beamline. Since the interaction region is located beyond the end of the optical table, also large detection chambers with special requirements like accessibility from the bottom or extended height can be used. Figure 1 shows the attosecond beamline with a magnetic-bottle-time-of-flight spectrometer for gaseous and liquid samples, which is described in detail and characterized in a different publication.[29]

III. ACTIVE STABILIZATION

To ensure attosecond stability in pump-probe experiments, an active stabilization of the optical path lengths is needed. A schematic overview of the stabilization system is shown in Figure 3. Unfortunately, there is no direct way to determine the delay between XUV and fundamental radiation, using the two different wavelengths. Therefore, an interferometer on a separate beam path is added above the main beam path using 1/2 in. optics. The mounts are joined to ensure that both beam paths are mechanically coupled and positioned as close to each other as possible to minimize the effect of mechanical vibrations. Two beams are propagating over the same optical surfaces: an intensity-stabilized helium-neon laser (Spectra Physics 117A) and a white-light beam generated by a fiber-coupled halogen light bulb (Osram Xenophot HLX 150W).

A. Helium-neon laser interferometry

Helium-neon laser interferometry is a very precise method to measure small changes in distances, but the interference signal is periodic in path-length difference, and therefore, absolute distances cannot be measured. Furthermore, the obtained interference signal is not linear with respect to the path-length difference of the two interfering paths, which makes active stabilization difficult. To overcome this, we use a quadrature detection scheme, which is schematically shown in Figure 3 (red beam path). In one arm of the interferometer, a half-wave plate and a quarter-wave plate are introduced to generate a circularly polarized beam and to compensate for ellipticity introduced by grazing-incidence reflections on metallic surfaces. The overlapping linearly and circularly polarized beams are propagated through a polarizing beam splitter and thereby split into two interference signals which are 90° out of phase. Both signals are detected with photodiodes that are read out by a National Instruments LabVIEW real-time computer system. A reference scan over several interference fringes allows for the determination of calibration factors which are given by the overall signal intensity on each photodiode and the modulation depth of the interference signal. Those factors are stored and used in the subsequent stabilization process to determine a phase angle. The angle Φ is calculated from the inverse tangent of the normalized (-1 to 1) photodiode signals (I_1, I_2): $\tan \Phi = I_1/I_2$. A software feedback-control loop which is processing the incoming data with a sampling rate of 30 kHz calculates and stabilizes this phase. Due to its linear dependence on the path-length difference, a stabilization to arbitrary positions on the delay axis is possible with the same control-loop parameters. The correction signal is frequency selected in the software and converted into two analog output signals. DC-components and low frequencies are fed to the two long-range piezo-stages, and the higher frequency components are directed through a fast amplifier to the small beam shifting piezo. An additional fringe counter is incorporated in the software.

B. White-light interferometry

The described helium-neon laser interferometer does not give any information about the absolute delay between the two pulses. In contrast, white-light interferometry provides this information. The interfering white-light beams are coupled into a high-resolution spectrometer (Ocean Optics HR4000, 0.24 nm resolution). The periodicity of the interference fringes in frequency space is directly related to the absolute path-length difference. Fourier transformation gives direct access to this quantity. An additional glass plate in one of the interferometer arms makes sure that the white light in both pathways experiences the same amount of dispersion.

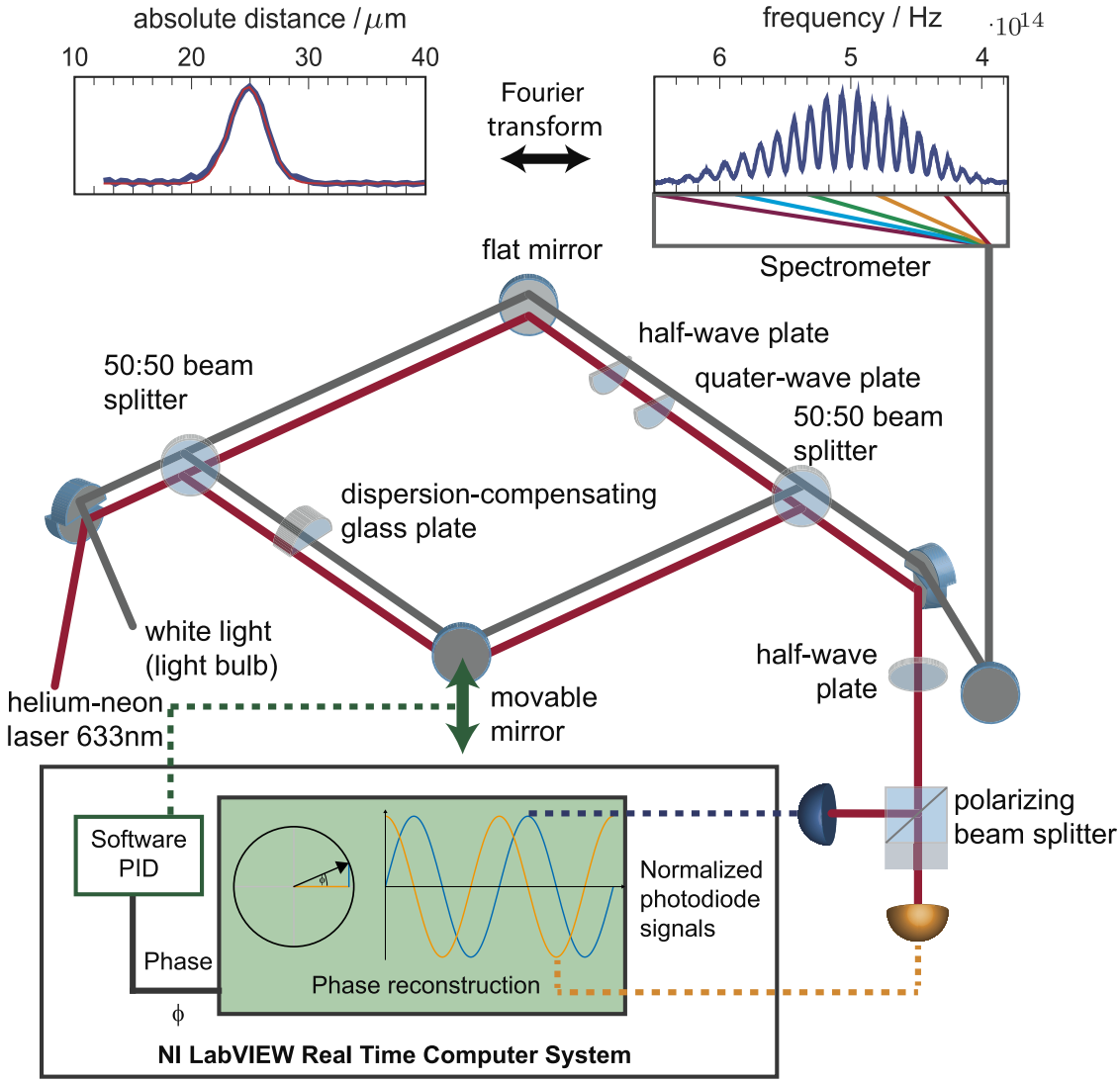

FIG. 3. Schematic drawing of reference interferometer and feedback loop for active stabilization.

The path-length difference in the stabilization beam path is chosen to be slightly (about 100 μm) different from the main beam path, since the interference pattern disappears at equal lengths. The signal extracted from the white-light interferometer cannot be used for the fast feedback loop due to the long (100 ms) integration time of the spectrometer. It is, however, a very convenient tool to find and preserve the temporal overlap of the pulses in the main beam path.

C. Short- and long-term stability

A successful attosecond experiment requires stable delay conditions over the duration of the experiment, which is typically on the order of one to several hours. Slow drifts during the measurement lead to a distorted delay axis. To resolve features on the attosecond time scale the short-term stability and the spectral composition of the path-length fluctuations are the limiting factors. These quantities are measured by a photodiode that detects the interference between the IR beam and the residual IR which is propagating through the XUV beam path when no metallic filter is used. The signal is acquired for one second during which one arm of the interferometer is blocked at every second acquisition by the optical chopper. This allows for normalization of the interference signal to compensate laser intensity fluctuations. The interferometer is scanned over several fringes before each stability measurement to quantify the modulation depth and determine calibration factors. A typical long-term drift behavior without active stabilization is shown in Figure 4(a), which results in a peak-to-peak drift of 300 as over two hours and a good passive stability of 41 as ± 24 as rms. The confidence interval (95%) is determined by the standard deviation of three independent measurements and accounts for daily differences in the vibrational noise level of the laboratory environment. The corresponding signal from the white-light interferometer is plotted in the same panel and shows that the behavior of the two beam paths is very similar. The same out-of-loop measurement was repeated seven times with active stabilization, which results in a root-mean-square deviation and a 95% confidence interval of 26 as ± 10 as. A

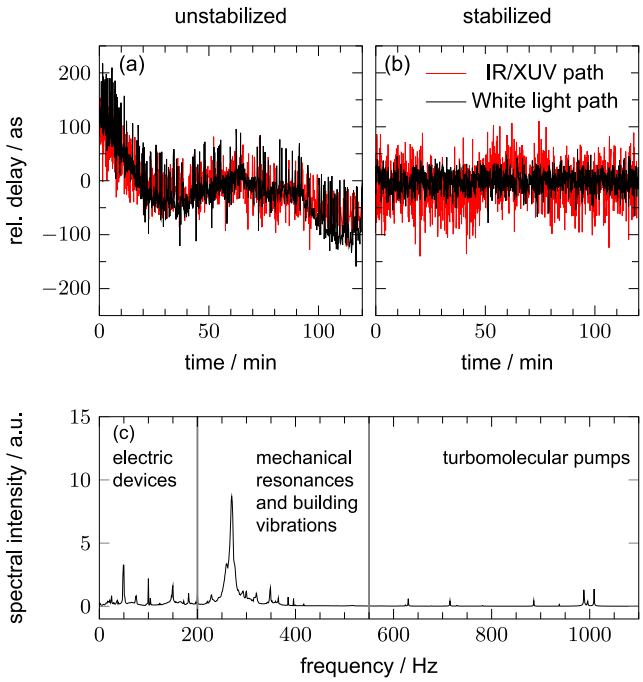

FIG. 4. Relative delay in the lower beam path (XUV/IR) and in the upper beam path (white-light) measured for the free-running case (a) and for the actively stabilized case (b). The bottom panel (c) shows a spectrum of the short-term path-length fluctuations measured in the helium-neon-laser-signal.

typical measurement is shown in Figure 4(b). The short term stability and its spectral composition are measured using the helium-neon-laser interferometer because, in contrary to the IR laser, it can be sampled with 30 kHz. A spectrum of the vibrations is shown in Figure 4(c). The region up to 200 Hz is dominated by 50 Hz and its overtones, which originate from various devices in the building running at the frequency of the power grid. The dominating group of peaks around 300 Hz represents mechanical resonances of the mirror mounts and the vacuum setup and also includes vibrations which are present throughout the building and could be measured with an accelerometer-based vibration sensor as well. The higher frequency components can be directly assigned to the vacuum pumps attached to the setup. They can be characterized by looking at one-second time-intervals of the in-loop error signal of the helium-neon-laser interferometer. The root-mean-square deviation corresponding to the spectrum shown in Figure 4(c), is 48.6 as ± 0.4 as. The mean value and confidence interval (95%) result from 650 measurements, distributed over one night.

IV. APPLICATION

An application which requires high temporal stability is the characterization of attosecond pulse trains. The detection of photoelectrons generated by an XUV pulse train and a weak IR field, which are delayed with respect to each other, allows for the reconstruction of the attosecond pulses within the pulse train. The weak IR field generates sidebands between the photoelectron peaks originating from the XUV pulse train. Two quantum paths (harmonic order plus IR photon and harmonic order minus IR photon) result in electrons at the same kinetic energies, and therefore, they can interfere, which leads to an oscillating intensity of the sidebands while scanning the IR-XUV-delay. The method is known as Reconstruction of Attosecond Bursts by Interference of Two-photon Transitions (RABITT).[7] A typical RABITT-trace, where high-order-harmonic generation from 800 nm is performed in neon and the photoelectrons emitted from argon are detected, is shown in Figure 5(a). The residual infrared light propagating along the XUV-path is blocked by a 100 nm thick aluminium filter. The experimental data converted to photoelectron kinetic energy are shown in the main panel. The right panel shows a difference spectrum (XUV+IR minus XUV only) at maximum sideband intensity. Positive contributions are due to sidebands generated by the presence

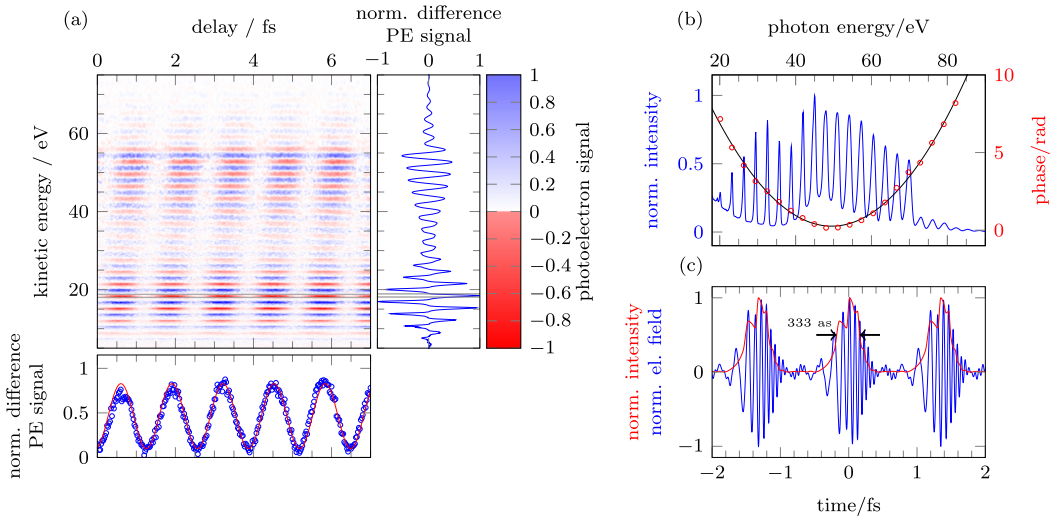

FIG. 5. (a) RABITT trace in argon recorded with 25 as delay steps. The high-order harmonics were generated in neon. The lower panel shows the integrated signal of sideband 22. The right panel shows a difference spectrum (XUV+IR minus XUV only) at maximal intensity of sideband 22. Positive contributions are sidebands, negative contributions are depletion of XUV-induced photoelectron peaks. (b) Ionization cross section[24] corrected photoelectron (PE) spectrum and reconstructed spectral phase, including the correction due to the atomic phase of argon.[30] The black line shows a quadratic fit to the retrieved phase. (c) Reconstructed XUV time trace: electric field (blue) and intensity profile (red).

of the infrared laser field, and negative contributions are depletion of the photoelectrons generated by the XUV-pulse-train alone. The shot-to-shot referencing using the optical chopper reduces the effect of XUV intensity fluctuations. The spectrum is integrated over the energy range of sideband 22 and shown in the lower panel. Fourier transformation or time-domain-fitting (shown in red) allows for the determination of the phase of the sideband oscillation of all sidebands. The achieved modulation depth of almost 100% indicates good spatial and temporal overlap between the two independent imaging systems. The spectrum of the XUV radiation can be retrieved from the photoelectron time-of-flight signal by converting it to electron kinetic energy, while maintaining the peak integrals (Jacobi correction) and correcting for the energy-dependent photoionization cross section of the detection gas. The spectral amplitude and phase are shown in Fig. 5(b). The spectral phase is retrieved from the sideband oscillations of the RABITT-trace and corrected for the contribution of the atomic phase of argon, using theoretical values.[30] From these quantities, an average XUV pulse within the pulse train can be calculated. The temporal electric field (blue) and intensity profile (red) are shown in panel (c) and result in a full-width-half-maximum (FWHM) of 333 as.

V. SUMMARY

We have shown that our attosecond beamline allows for measurements with high temporal resolution. The remaining path-length drifts and instabilities were minimized through active stabilization. The choice of spatially separated beam paths with separate imaging systems makes the beamline versatile but still compact. It especially allows for single-shot-referenced pump-probe measurements to detect small changes on a background. The white-light interferometric measurement gives an absolute path-length difference and makes it straightforward to find temporal overlap of the XUV and IR pulses. The high broadband XUV-reflectivity and the compatibility of the beamline with a wide range of detectors and different high-harmonic sources open a variety of experiments in multiple energy- and pulse-duration regimes such as RABITT, streaking or transient-absorption measurements.

ACKNOWLEDGMENTS

The research presented in this publication has received funding from the European Research Council (ERC) under the European Union's Seventh Framework Programme (FP/2007-2013)/ERC Grant Agreement No. 307270-ATTOSCOPE and from ETH Zurich (ETH Independent Investigators' Research Awards (ETHIIRA, No. ETH-41 11-2)).

We thank Ulrich Müller from the Swiss Federal Laboratories for Materials Science and Technology (EMPA) for the carbon coating of our XUV-mirrors and the preceding discussions. Special thanks goes to our electronic and mechanical workshops within ETH/D-CHAB for excellent work contributed to this research project. In particular, we want to thank Markus Steger, Andreas Schneider, and Andrés Laso.

[1]M. Drescher, M. Hentschel, R. Kienberger, M. Uiberacker, V. Yakovlev, A. Scrinzi, T. Westerwalbesloh, U. Kleineberg, U. Heinzmann, and F. Krausz, "Time-resolved atomic inner-shell spectroscopy," Nature **419**, 803–807 (2002).

[2]F. Calegari, D. Ayuso, A. Trabattoni, L. Belshaw, S. De Camillis, S. Anumula, F. Frassetto, L. Poletto, A. Palacios, P. Decleva, J. B. Greenwood, F. Martín, and M. Nisoli, "Ultrafast electron dynamics in phenylalanine initiated by attosecond pulses," Science **346**, 336–339 (2014).

[3]S. Neppl, R. Ernstorfer, A. L. Cavalieri, C. Lemell, G. Wachter, E. Magerl, E. M. Bothschafter, M. Jobst, M. Hofstetter, U. Kleineberg, J. V. Barth, D. Menzel, J. Burgdörfer, P. Feulner, F. Krausz, and R. Kienberger, "Direct observation of electron propagation and dielectric screening on the atomic length scale," Nature **517**, 342–346 (2015).

[4]M. Drescher, M. Hentschel, R. Kienberger, G. Tempea, C. Spielmann, G. A. Reider, P. B. Corkum, and F. Krausz, "X-ray pulses approaching the attosecond frontier," Science **291**, 1923–1927 (2001).

[5]M. Schultze, A. Wirth, I. Grguras, M. Uiberacker, T. Uphues, A. J. Verhoef, J. Gagnon, M. Hofstetter, U. Kleineberg, E. Goulielmakis, and F. Krausz, "State-of-the-art attosecond metrology," J. Electron Spectrosc. Relat. Phenom. **184**, 68–77 (2011).

[6]F. M. Böttcher, B. Manschwetus, H. Rottke, N. Zhavoronkov, Z. Ansari, and W. Sandner, "Interferometric long-term stabilization of a delay line: A tool for pump-probe photoelectron-photoion-coincidence spectroscopy on the attosecond time scale," Appl. Phys. B **91**, 287–293 (2008).

[7]P. M. Paul, E. S. Toma, P. Breger, G. Mullot, F. Auge, P. Balcou, H. G. Muller, and P. Agostini, "Observation of a train of attosecond pulses from high harmonic generation," Science **292**, 1689–1692 (2001).

[8]H. Mashiko, M. J. Bell, A. R. Beck, M. J. Abel, P. M. Nagel, C. P. Steiner, J. Robinson, D. M. Neumark, and S. R. Leone, "Tunable frequency-controlled isolated attosecond pulses characterized by either 750 nm or 400 nm wavelength streak fields," Opt. Express **18**, 25887–25895 (2010).

[9]H. Mashiko, M. J. Bell, A. R. Beck, D. M. Neumark, and S. R. Leone, "Frequency tunable attosecond apparatus," Prog. Ultrafast Intense Laser Sci. **106**, 49–63 (2014).

[10]S. J. Weber, B. Manschwetus, M. Billon, M. Böttcher, M. Bougeard, P. Breger, M. Géléoc, V. Gruson, A. Huetz, N. Lin, Y. J. Picard, T. Ruchon, P. Salières, and B. Carré, "Flexible attosecond beamline for high harmonic spectroscopy and XUV/near-IR pump probe experiments requiring long acquisition times," Rev. Sci. Instrum. **86**, 033108 (2015).

[11]D. Guénot, D. Kroon, E. Balogh, E. W. Larsen, M. Kotur, M. Miranda, T. Fordell, P. Johnsson, J. Mauritsson, M. Gisselbrecht, K. Varjù, C. L. Arnold, T. Carette, A. S. Kheifets, E. Lindroth, A. L'Huillier, and J. M. Dahlström, "Measurements of relative photoemission time delays in noble gas atoms," J. Phys. B: At., Mol. Opt. Phys. **47**, 245602 (2014).

[12]D. Kroon, D. Guénot, M. Kotur, E. Balogh, E. W. Larsen, C. M. Heyl, M. Miranda, M. Gisselbrecht, J. Mauritsson, P. Johnsson, K. Varjú, A. L'Huillier, and C. L. Arnold, "Attosecond pulse walk-off in high-order harmonic generation," Opt. Lett. **39**, 2218–2221 (2014).

[13]G. Gademann, F. Kelkensberg, W. K. Siu, P. Johnsson, M. B. Gaarde, K. J. Schafer, and M. J. J. Vrakking, "Attosecond control of electron-ion recollision in high harmonic generation," New J. Phys. **13**, 033002 (2011).

[14]G. Sansone, E. Benedetti, F. Calegari, C. Vozzi, L. Avaldi, R. Flammini, L. Poletto, P. Villoresi, C. Altucci, R. Velotta, S. Stagira, S. De Silvestri, and M. Nisoli, "Isolated single-cycle attosecond pulses," Science **314**, 443–446 (2006).

[15]M. Chini, H. Mashiko, H. Wang, S. Chen, C. Yun, S. Scott, S. Gilbertson, and Z. Chang, "Delay control in attosecond pump-probe experiments," Opt. Express **17**, 21459–21464 (2009).

[16]R. Locher, M. Lucchini, J. Herrmann, M. Sabbar, M. Weger, A. Ludwig, L. Castiglioni, M. Greif, M. Hengsberger, L. Gallmann, and U. Keller, "Versatile attosecond beamline in a two-foci configuration for simultaneous time-resolved measurements," Rev. Sci. Instrum. **85**, 013113 (2014).

[17]M. Fiess, M. Schultze, E. Goulielmakis, B. Dennhardt, J. Gagnon, M. Hofstetter, R. Kienberger, and F. Krausz, "Versatile apparatus for attosecond metrology and spectroscopy," Rev. Sci. Instrum. **81**, 093103 (2010).

[18]A. McPherson, G. Gibson, H. Jara, U. Johann, and T. S. Luk, "Studies of multiphoton production of vacuum-ultraviolet radiation in the rare gases," J. Opt. Soc. Am. B: Opt. Phys. **4**, 595–601 (1987).

[19]M. Ferray, A. L'Huillier, X. F. Li, L. A. Lompre, G. Mainfray, and C. Manus, "Multiple-harmonic conversion of 1064 nm radiation in rare gases," J. Phys. B **21**, L31–L35 (1988).

[20]J. R. Sutherland, E. I. Christensen, N. D. Powers, S. E. Rhynard, J. C. Painter, and J. Peatross, "High harmonic generation in a semi-infinite gas cell," Opt. Express **12**, 4430 (2004).

[21]J.-P. Brichta, M. C. H. Wong, J. B. Bertrand, H.-C. Bandulet, D. M. Rayner, and V. R. Bhardwaj, "Comparison and real-time monitoring of high-order harmonic generation in different sources," Phys. Rev. A **79**, 33404 (2009).
[22]A. F. von Conta, M. Huppert, and H. J. Wörner, "A table-top monochromator for tunable high-harmonic femtosecond XUV pulses" (to be published).
[23]H.-J. Hagemann, W. Gudat, and C. Kunz, "Optical constants from the far infrared to the x-ray region: Mg, Al, Cu, Ag, Au, Bi, C, and Al_2O_3," J. Opt. Soc. Am. **65**, 742 (1975).
[24]B. L. Henke, E. M. Gullikson, and J. C. Davis, "X-ray interactions: Photoabsorption, scattering, transmission and reflection at e = 50-30 000 eV, Z = 1-92," At. Data Nucl. Data Tables **54**, 181–345 (1993).
[25]M. Fushitani, A. Matsuda, and A. Hishikawa, "Time-resolved EUV photoelectron spectroscopy of dissociating I_2 by laser harmonics at 80 nm," Opt. Express **19**, 9600–9606 (2011).
[26]W. R. Hunter, D. W. Angel, and R. Tousey, "Thin films and their uses for the extreme ultraviolet," Appl. Opt. **4**, 891 (1965).
[27]F. R. Powell, P. W. Vedder, J. F. Lindblom, and S. F. Powell, "Thin film filter performance for extreme ultraviolet and x-ray applications," Opt. Eng. **29**, 614–624 (1990).
[28]R. López-Martens, K. Varjú, P. Johnsson, J. Mauritsson, Y. Mairesse, P. Salières, M. B. Gaarde, K. J. Schafer, A. Persson, S. Svanberg, C.-G. Wahlström, and A. L'Huillier, "Amplitude and phase control of attosecond light pulses," Phys. Rev. Lett. **94**(3), 033001 (2005).
[29]I. Jordan, M. Huppert, M. A. Brown, J. A. van Bokhoven, and H. J. Wörner, "Photoelectron spectrometer for attosecond spectroscopy of liquids and gases," Rev. Sci. Instrum. (to be published).
[30]J. Mauritsson, M. B. Gaarde, and K. J. Schafer, "Accessing properties of electron wave packets generated by attosecond pulse trains through time-dependent calculations," Phys. Rev. A **72**, 013401 (2005).